IOSR Journal of Electronics and Communication Engineering (IOSR-JECE)
e-ISSN: 2278-2834, p- ISSN: 2278-8735.Volume 21, Issue 2, Ser. 1 (Mar – Apr 2026), PP 29-37
www.iosrjournals.org

Multi-Objective Design And Optimisation Of A Three-Phase Induction Motor For Traction Application

Asuquo Eke, O.I. Okoro, A. J. Onah
Department Of Electrical/Electronic Engineering, Cross River University Of Technology, Calabar. Nigeria
Department Of Electrical/Electronic Engineering, Michael Okpara University Of Agriculture, Umudike. Abia State. Nigeria
Department Of Electrical/Electronic Engineering, Michael Okpara University Of Agriculture, Umudike. Abia State. Nigeria

Abstract
In contemporary electric drive systems, where high efficiency, lower current consumption, and enhanced torque output are crucial, the design and performance optimization of three-phase induction motors for traction applications have grown in importance. The results of this study's application of the multi-objective optimization (MOO) approach to induction motor design are contrasted with those of conventional motor design, single-objective optimization (SOO), and experimental measurements. Important performance metrics, such as output power, torque, efficiency, and stator current, were taken into account during the optimization process. While the original motor design achieved small improvements with 3.5 A, 75% efficiency, 14.2 Nm torque, and 1.5 W output, the experimental evaluation revealed a current draw of 3.8 A, efficiency of 72%, torque of 14.1 Nm, and power output of 1.5 W. With a lower current of 3.2 A, increased efficiency of 85%, and a notable torque increase to 45 Nm, the motor further improved under SOO, proving the value of single-criterion optimization. Superior performance enhancements were offered by MOO, though, which maintained a low operating current while producing a significant increase in torque to 65 Nm, efficiency above 90%, and power output far beyond 1.5 W. The findings demonstrate the effectiveness of multi-objective optimization in resolving parameter conflicts and producing an overall optimal design appropriate for traction applications. This study sheds light on the function of sophisticated optimization algorithms in the design of electric machines and shows that MOO can produce induction motors with increased torque density, efficiency, and lower current demand, improving their suitability for electrified vehicles and sustainable transportation.

Keyword: *Three-Phase Induction Motor, Multi-Objective Optimization, Traction Applications, Motor Design*

Date of Submission: 16-03-2026 Date of Acceptance: 26-03-2026

I. Introduction

Because of their affordability, dependability, and ease of use, induction motors are widely used across a range of sectors and applications. Developing a device that effectively transforms electrical energy into mechanical energy is the goal of induction motor design. According to Shaikh et al. (2022), this procedure is based on the electromagnetic induction principles. Asynchronous speed machines are induction machines. They are operated by either a motor or a generator. Compared with other motors, it is less costly than equivalent synchronous or DC machines. Because of its low maintenance costs, durability, and straightforward construction, it is regarded as a workhorse in the industrial sector. Induction machines are used in a wide range of commercial, residential, and industrial settings [1, 2]. Researchers have been interested in the use of these machines for traction applications, which will help reduce costs and require less maintenance. A lot of work has been done on the design and optimization of these machines. In this work, the design and multiobjective optimization of this machine for traction applications are studied. These new motor design configurations and techniques have the potential to improve the performance of these machines and increase their efficiency and reliability [8]. The main objective of designing an induction motor is to ascertain the precise physical dimensions of each component in order to satisfy customer demands. The following design details are required: the stator's main dimensions, the stator winding details, the rotor's design details and its windings, and performance characteristics. [3, 4] state that when building a motor using the standard magnetic circuit method, it is necessary to provide certain initial assumed values for circuit parameters and geometric parameters according to the performance. The designer needs the client's specifications in order to obtain the design details, which include the following: rated output power, designed voltage, number of phases, speed, frequency range, connection of stator winding, type of rotor winding, working conditions, shaft extension details, etc. In addition to the aforementioned, the designer needs information about the design equations that determine how the design procedure is set up, details about the different options

for different parameters, details about the availability of different materials, and the limiting values of various performance parameters like iron and copper losses, no load current, power factor, temperature increase, and efficiency [5]. According to [6] when designing an induction motor to optimize its performance in terms of efficiency, power factor, torque output, and reliability, it involves careful consideration of various parameters, since the parameters are conflicting in nature. For instance, while optimizing for efficiency, the results may alter the torque density; one needs to be careful when picking the parameters to be improved. A generic algorithm was applied in [6] using T-type equivalent circuit that uses geometry variables in the design, which gives a good performance forecasting ability. The targeted aims or objectives are increasing power density and decreasing the cost of manufacturing in the frontier mode software. The thermal aspect of the motor was also addressed, while temperature matching of different components of the motor, the motor has a standing ambient temperature of 313-1k for optimum design. Design optimization was done utilizing the analysis manual as a tool. The program will configure the geometry parameters used by this tool based on the provided parameters. According to [7, 8], claim that a two-degree-of-freedom motor's efficiency is worse because of its increased losses. Its primary use is in rotor optimization, which takes the rotary armature size limitation into account. This contributes to the improved performance and efficiency of the motor suggested by the Taguchi technique optimization. A permanent magnet synchronous motor with a power of 2MW and a solution in electromagnetic, thermal, and mechanical aspects parametric model generated based on the finite element method (FEM) was studied by [10] using a multi-objective genetic algorithm. With a copper loss of 11862W and an iron loss of 5720. 5w, the efficiency increased to 99.13% [11]. A Motorcad white paper from 2021 described the design and optimization of a 200V induction motor for traction purposes. uses a simulation tool that makes use of motor-cad and optislang. To achieve the motor's peak and continuous performance, both thermal and electromagnetic optimization were done. They introduced the two-stage optimization. Optislang considers mood goods (objectives) and does multi-objective optimization. The work's objective was to increase torque and efficiency while lowering the motor's weight and cost. The meta-model approach was the method used [12, 13, 14, 15].

II. Methodology

The technique for multi-objective design and optimization of a three-phase induction motor (IM) for traction applications follows a systematic, iterative, and coupled electro-thermal technique. The process integrates electromagnetic design, thermal evaluation, constraints, and optimization algorithms to attain competing overall performance objectives under actual traction operating conditions. Induction motor design is as follows.

The stator bore diameter of the SCIM is given according to [1, 2, 4, 15]

$$D_{is(SCIM)} = \sqrt[3]{\frac{2\mathcal{P}_1^2 S_{gap}}{\pi\lambda f C_0}}, \quad (1)$$

where pole pairs, apparent airgap power, aspect ratio, supply frequency, and Esson's constant (147 × 103 J/m3) are represented by the variables p1, Sgap, λ, f, and C0, respectively.

For dimensioning the SCIM, the following formulas are used to get the pole pitch, τ(SCIM), stack length, Lst(SCIM), and slot pitch,

$$\tau\text{s(SCIM)}: \tau_{(SCIM)} = \frac{\pi D_{is(SCIM)}}{2\mathcal{P}_1}, L_{st(SCIM)} = \lambda\tau_{(SCIM)}, \tau_{s(SCIM)} = \frac{\tau_{(SCIM)}}{3q}. \quad (2)$$

The aspect ratio, pole pitch, and stator slots per pole are respectively represented as λ, $\tau_{(SCIM)}$, and q, whereas the stator outer diameter, $D_{os(SCIM)}$, airgap length, and rotor outer diameter are approximated as follows:

$$D_{os(SCIM)|} = \frac{D_{is(SCIM)}}{0.62}, \quad (3)$$

$$g_{(SCIM)} = (0.1 + 0.012 \times \sqrt[3]{P_n}), \quad (4)$$

$$D_{or(SCIM)} = D_{is(SCIM)} - g_{(SCIM)}. \quad (5)$$

The rated power is given by P_n. The determination of the number of turns per phase, W_1, depends on the airgap flux density, $B_{g(SCIM)}$, and is done as follows:

$$W_1 = \frac{0.22V_{(SCIM)}}{K_{w1} f a_i \tau_{(SCIM)} L_{st(SCIM)} B_{g(SCIM)}}, \quad (6)$$

where V_{SCIM}, K_{w1}, and α_i, stand for supply voltage, stator winding factor, and pole spanning coefficient, respectively. The number of conductors per slot, $n_{c(SCIM)}$, is given as:

$$n_{c(SCIM)} = \frac{a_1 w_1}{p_1 q}. \quad (7)$$

A_1 represents the number of parallel current pathways. It should be noted that because a double-layer winding includes two distinct coils in each slot, an even number of slots is necessary. The definitions of the wire gauge diameter (d_{co}) and rated current (I_{in}) are as follows:

$$I_{in} = \frac{P_n}{n\cos(\phi)\sqrt{3}V_{SCIM}}, \quad (8)$$

$$D_{co} = \sqrt{\frac{2I_{in}}{\pi a_p J_{(SCIM)}}}, \quad (9)$$

where a_p,$J_{(SCIM)}$, and η represent conductors in parallel, current density, and efficiency, respectively.

Assuming all the airgap flux passes through the stator teeth, the useful slot area, A_{su}, and stator tooth width, b_{ts}, are respectively given as:

$$A_{su} = \frac{\pi d_{co}^2 a_p n_{c(SCIM)}}{4K_{fill}}, \quad (10)$$

$$b_{ts} = \frac{B_{g(SCIM)}\tau_{(SCIM)}}{0.96B_{ts}}. \quad (11)$$

The fill factor and stator tooth flux density are as follows K_{fill} and B_{ts}, respectively. For stator slot sizing, the lower width, b_{s1}, higher width, b_{s2}, and slot height, h_s, are given as:

$$b_{s1} = \frac{\pi(D_{in(SCIM)}+2h_{os}+2h_w}{N_s} - b_{ts}, \quad (12)$$

$$b_{s2} = \sqrt{4A_{su}tan\frac{\pi}{N_s} + b_{s1}^2}, \quad (13)$$

$$h_{s2} = \frac{2A_{su}}{b_{s1}+b_{s2}}. \quad (14)$$

The lower slot height, wedge height, slot effective area, and number of stator slots are denoted as h_{os}, h_W, A_{su}, and N_s, respectively. If stator and rotor teeth give the same effects, the teeth saturation factor ($1 + K_{st}$) is calculated as follows:

$$1 + K_{st} = \frac{1+F_{mts}+F_{mtr}}{F_{mg}}, \quad (15)$$

where F_{mts}, F_{mtr}, and F_{mg} represent stator tooth, rotor tooth, and airgap MMFs, respectively. The end-ring current, I_{er}, and magnetization current, I_μ, are respectively calculated as follows

$$I_{er} = \frac{1_b}{2sin\left(\frac{\pi p_1}{N_r}\right)}, \quad (16)$$

$$I_\mu = \frac{\pi p_1 \left(F/_2\right)}{\sqrt[3]{2}W_1 K_{w1}}, \quad (17)$$

where I_b, Nr, and F are the rotor bar current, the number of rotor slots, and the magnetization MMF, respectively. For the rotor slot sizing, the rotor slot pitch, τ_r, and tooth width, b_{tr}, are respectively calculated as:

$$\tau_r = \frac{\pi(D_{in(SCIM)}-2g_{(SCIM)})}{N_r}, \quad (18)$$

$$b_{tr} = \frac{\tau_r B_{g(SCIM)}}{0.96Bt_r}. \quad (19)$$

The rotor tooth flux density is represented as B_{tr}. The rotor slot geometry is obtained by using the slot area, A_b, equation given as follows:

$$A_b = \frac{\pi}{8}(d_1^2 + d_2^2) + \frac{(d_1+d_2)h_r}{2}. \quad (20)$$

The diameters d_1 and d_2 are obtained simultaneously from

$$d_1 = \frac{\pi(D_{re}-2h_{or})-N_r b_{tr}}{\pi+N_r} \; and \; d_1 - d_2 = 2h_r tan\frac{\pi}{N_r}. \quad (21)$$

The symbols Dor (SCIM), hr, hcr, and hor stand for the rotor's outer diameter, rotor slot height, rotor back core height, and lower rotor slot height, respectively. The following method yields the shaft's greatest diameter or D-shaft.:

$$\left(D_{shaft}\right)_{maxb} \leq D_{is(SCIM)} - 2g_{(SCIM)} - 2\left(h_{or} + \frac{d_1+d_2}{2} + h_r + h_{cr}\right). \quad (22)$$

Considering mechanical design concerns and prior knowledge, the rated torque dictates the choice of shaft diameter. It is imperative to stress that in the event that these criteria fail to satisfy the design goals, they will be recalculated. The stator resistance, stator inductive reactance, magnetizing reactance, core loss component, rotor resistance referred to stator, rotor resistance, rotor inductive reactance referred to stator, transformation ratio, and load resistance referred to the stator are represented as Rs, Xs, Xm, Rc, $R\}$r, Rr, $X\}$r, Xr, K, and $R\}$r . These factors help determine performance metrics like power factor, rated torque, rated slip, efficiency, and the magnetization behavior of the motor. The stator and rotor phase parameters are provided as:

$$R_s = \frac{\rho_{co} L_c W_1}{A_{co} a_1}, \quad (23)$$

$$X_s = \frac{2\mu_0 \omega_1 L W_1^2 (\lambda_s+\lambda_{ds}+\lambda_{ec})}{p_1 q} \quad (24)$$

$$R_r = \frac{4m(W_1 K_{w1})^2 R_{be}}{N_r} \quad (25)$$

$$X_r = \frac{4m(W_1 K_{w1})^2 X_{be}}{N_r} \quad (26)$$

while the magnetizing reactance is computed as:

$$X_m = \sqrt{\left(\frac{V_{SCIM}}{I_\mu}\right)^2 - R_s^2 - X_{sL}} \quad (27)$$

The symbols Lc, ρco, μ₀, Aco, λs, λds, λec, Rbe, and Xbe represent the coil length, copper resistivity, permeability of free space, magnetic wire cross-section, slot differential and end ring connection coefficients, equivalent rotor bar resistance and reactance, and phase rotor resistance, respectively. The rated slip s_n, starting current I_{str}, and starting torque T_{str} of the motor are respectively defined as:

$$S_n = \frac{P_{Al}}{P_n + P_{Al} + P_{mv} + P_{stray}} \quad (28)$$

$$I_{str} = \frac{V_{SCIM} - E_r^{'}}{jX_S} = \frac{V_{SCIM}}{\sqrt{R_S + R_r^{S=1^2} + \left(X_S + X_r^{S=1}\right)^2}} \quad (29)$$

$$T_{str} = \frac{3p_1 R_r^{S=1} I_{str}^2}{\omega_n} \quad (30$$

where P_{Al}, P_{mv}, and P_{stray} represent rotor cage losses, mechanical/ventilation losses, and stray losses, respectively. The power factor of the electrical motor is computed as:

$$PF = \frac{P_{in}}{3V_{rms}I_{rms}} = cos(\theta_v - \theta_i) \quad (31)$$

where P_{in} is the input power of the motor, I_{rms} and V_{rms} are the root mean square (RMS) values of both the current (I_S) and voltage (V_{SCIM}), while θv and θi are the phases of voltage and current, respectively.

On the other hand, the rated shaft torque, T_n, and torque ripple, T_R, are respectively computed as follows:

$$T_n = {P_n}\Big/{\frac{2\pi f}{p_1}}(1 - S_n) \quad (32)$$

$$TR = \frac{T_{max} - T_{min}}{T_{avg}} \quad (33)$$

where $T_{(max)}$ is the maximum torque, $T_{(min)}$ is the minimum torque, and T_{avg} is the average torque. While the motion equation is given as:

$$T_n - T_L = J\frac{d\omega_r}{dt} \quad (34)$$

where T_L is the load torque and J is the inertia constant. Based on the classical equation, the efficiency of the electrical machine is defined as:

$$\eta = \frac{P_{out}}{P_{in}} = \frac{P_{out}}{P_{out} + P_{loss}}, \quad (35)$$

with the P_{out} and total loss (P_{loss}) calculated as:

$$P_{out} = 3I_r^2 R_r\left(\frac{1-s}{s}\right) - P_{mv} - P_{stray} \quad (36)$$

$$P_{loss} = P_{cu} + P_{Al} + P_{iron} + P_{mv} + P_{stray} \quad (37)$$

where P_{cu} is the stator winding losses, and P_{iron} is the core loss

The core loss is computed based on the formula proposed by [12] as:

$$P_{iron} = 7.16\left(\frac{f}{50}\right)^{1.3} G_{ts} + 5.12\left(\frac{f}{50}\right)^{1.3} G_{yl} + 31.03\ 10^{-7} \quad (38)$$

where G_{ts}, G_{yl}, and G_{tr} stand for stator tooth, yoke, and rotor tooth masses, respectively. The other loss components are defined as:

$$P_{cu} = 3R_s I_{in}^2, P_{Al} = 3R_r I_{in}^2, P_{mv} = 0.001P_n, P_{stray} = 0.01P_n. \quad (39)$$

Three phase induction motor has been designed based on the specifications in Table 1.0.

TABLE 1.0: Design Specification of Induction Motor

S/No.	Parameter	Values
1	Rated power	1.5kw
2	Type	3-phase
3	Rated frequency	50Hz
4	Rated Voltage	380
5	Connection	Star

III. Optimization Of Three Phase Induction Motor Design Formulation

It inspired by social behavior of birds., Each "particle" represents a candidate solution, Velocity and position update rules

$$v_i^{t+1} = wv_i^t + c_1 r_1\left(p_{i,\text{best}} - x_i^t\right) + c_2 r_2\left(g_{\text{best}} - x_i^t\right) \quad (40)$$

$$x_i^{t+1} = x_i^t + v_i^{t+1} \quad (41)$$

w is Inertia weight, c1,c2 are Cognitive and social factors, r1 and r2 are Random numbers in [10, 11]. The design optimization of an induction motor can be expressed mathematically as follows: Find $X(x_1, x_2, \ldots\ldots, x_n)$ such that F(X) is a minimized/Maximized Subject to:

$g_j(X) \geq 0\ j = 1,2, \ldots\ldots m$ (42)

and

$x_{Li} \leq x_i \leq x_{Ui}\ i = 1,2, \ldots\ldots n$ (43)

where $X(x_1, x_2, \ldots\ldots, x_n)$ is the set of independent design variables with their lower and upper limits as X_{Li} and x_U, for all ' n ' variables. F(X) is the objective function to be optimized and $g_j(X)$ are the constraints imposed on the design? This is a single objective optimization. For multi-objectives optimization (MOO) for induction motor design involves optimizing multiple conflicting objectives, such as efficiency and starting torque. Starting current and cost. The Formulation is as follows [12, 13, 14, 17]

$F(X_i) = [f_1(X), f_2(X), \ldots, f_m(X)]$ (44)

Minimize/Maximize: [η, T/V, C] (45)

Subject to: [J ≤ J_max] (46)

Design variables: [D, L, N, d, Dr]

Objective Functions

Efficiency (η): Maximize efficiency to reduce energy losses.

η = (Pout / Pin) * 100% (47)

Starting Torque: Maximize starting torque

$\frac{((Isc))^2}{Ir} \times$ Slip at Full Load. (48)

Design Variables	Range
1. Stator diameter (Ds)	130-140 mm)
2. Stator length (Ls)	65-75 mm)
3. Number of turns (N)	50-65
4. Wire diameter (Wd)	0,5-2.0(mm)
5. Rotor bar (Dr)	28-32 mm)

Constraints

Current density = J ≤ J_max (51)

IV. Result And Discussion

The result from the design and simulation of the motor is presented where done using MOTORCAD and OPTISLANG and the results obtained for efficiency (%) against speed (rpm), torque (Nm) against speed(rpm), speed (rpm) against time (sec), power factor against speed, current (A) against time (sec) and torque (Nm) against time (sec) are shown in figure 1-5. The particle swarm is configured for 1000 estimated evaluations and 100 samples per iteration to solve this study. The maximum number of candidates is 5, and the maximum Pareto percentage is 70. The adopted multi-objective optimization design method is the Pareto optimal plot. The particle swarm is used in this method to generate a set of optimal solutions that satisfy the design constraints and the motor performance distribution map. The priorities are torque, efficiency, power factor, and total loss. As a result, the final option chosen will have better starting torque, high efficiency, integrity, and a good power factor.

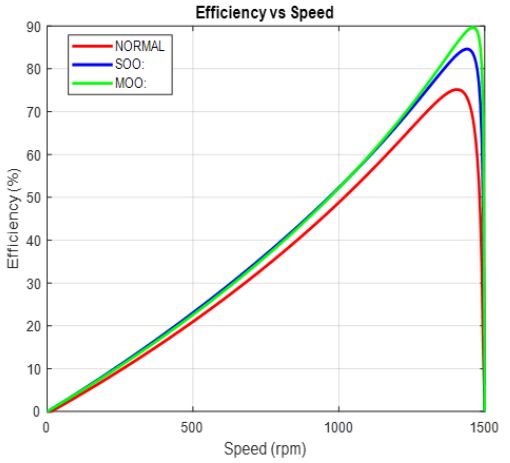

Figure1: Graph of efficiency against speed optimization (MOO)

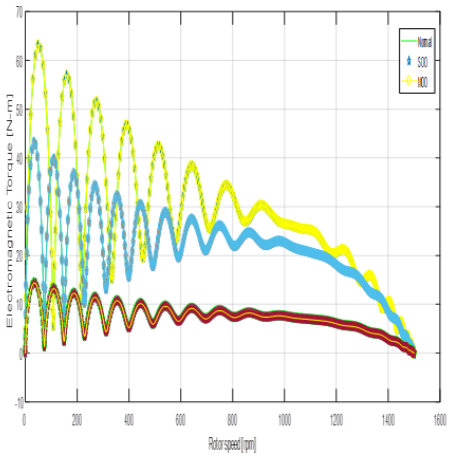

Figure2: Graph of Torque against (multi-objective Speed MOO

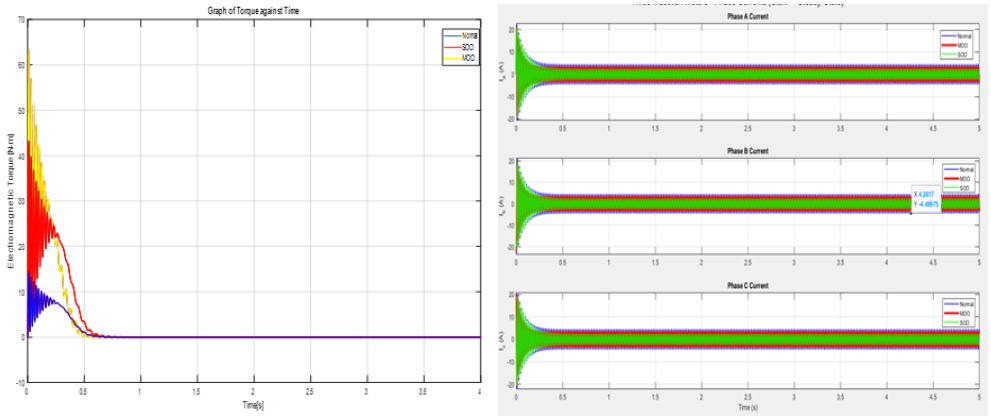

Figure 3: Graph of Torque against
Figure4: Graph of Current against Time (MOO) Time (MOO)

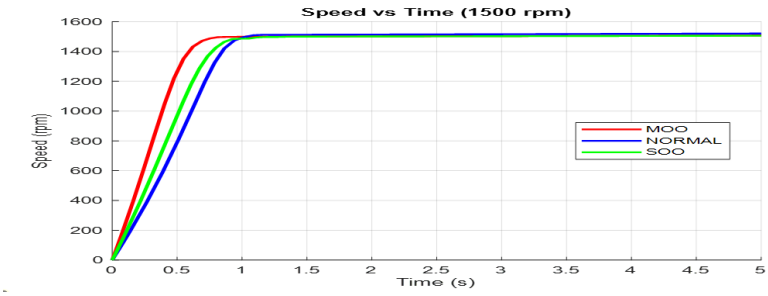

Figure 5: graph of Speed(rpm) against Times (sec) (MOO)

Figure 1 shows the motor efficiency values at the rated speed of 1495rpm for normal, SOO, and MOO as 74%, 83.3%, and 90.3%, respectively. Figure 2-3 shows torque values of 14.2 Nm, 44.0 Nm, and 64.0 Nm for normal, SOO, and MOO, respectively. Figure 4 has a starting current of 14.2A, 16.3A, and 23.0A, respectively, and stable current flow of 3.8A, 3.6A, and 3.0A, respectively, for normal, NOO, and MOO. Figure 5, the MOO has a faster stability, this is attained at 0.6s, for SOO is at 0.85s, and for Normal is at 1,1s.

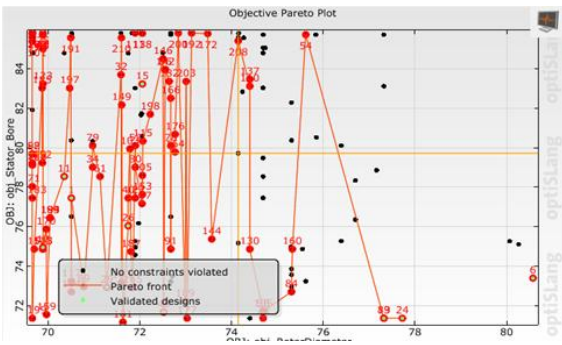

Figure 6: Rotor slot depth with design point

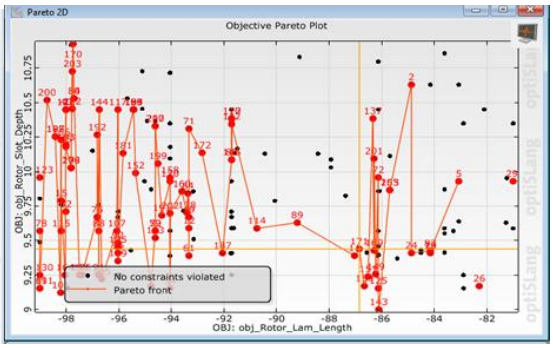

Figure 7: Stator bore with design point

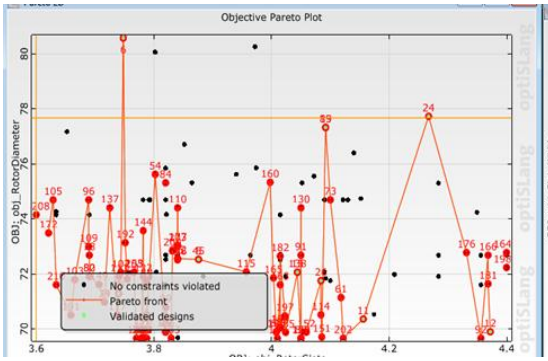

Figure: 8: Stator Width with design point

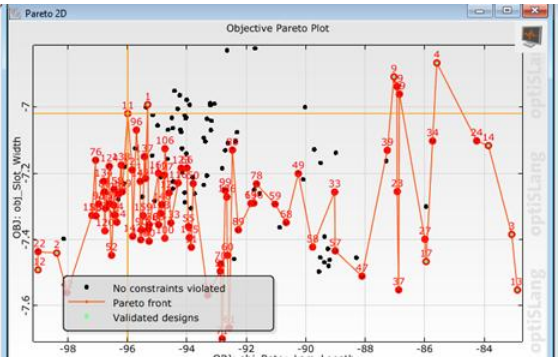

Figure:9: Rotor diameter with design point

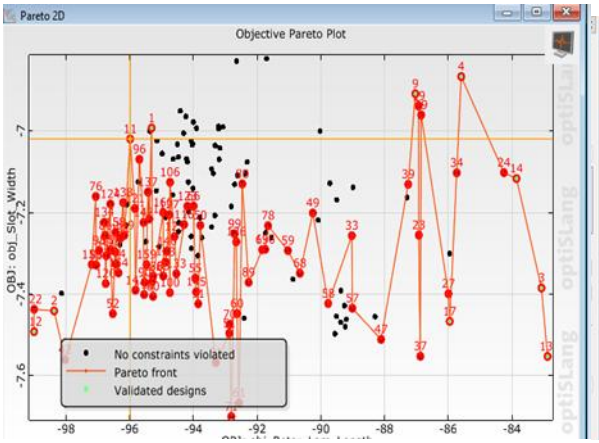

Figure 10: Rotor lam-length with slot width

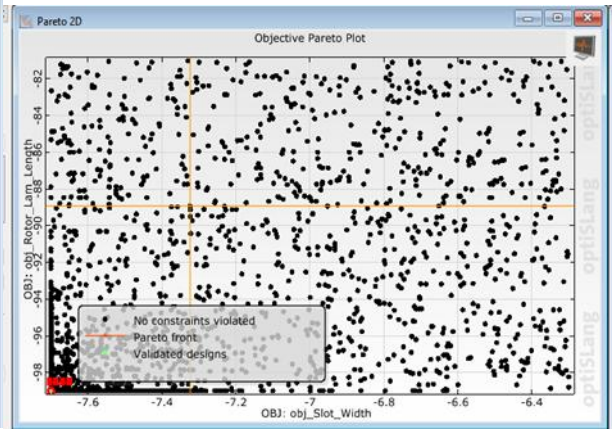

Figure 11: Rotor lam-length with slot width

The particle swarm is configured for 1000 estimated evaluations and 100 samples per iteration to solve this study. The maximum number of candidates is 5, and the maximum Pareto percentage is 70. The adopted multi-objective optimization design method is the Pareto optimal plot. The particle swarm is used in this method to generate a set of optimal solutions that satisfy the design constraints and the motor performance distribution map. The priorities are torque, efficiency, power factor, and total loss. As a result, the final option chosen will have higher starting torque, greater efficiency, integrity, and a good power factor. A black dot represents a design or solution evaluated during the optimization process. This corresponds to designs meeting all design constraints; the Pareto front is indicated by the red dot, which consists of non-dominated solutions. These are the "best possible trade-offs"; one cannot improve one objective without degrading the other. Green crosses: Indicate validated designs. These are designs that have been verified through detailed simulation or testing (higher fidelity models). They're sparse, suggesting only a few solutions were fully validated for the best model. The summary of motor performance is presented in Table 2.0 for the design and optimized models. Table 3.0 is the initial design and optimized design values of the motor variable. Figure 6 shows the relationship between stator bore dimension (x-axis) and objective function value. Stator bore with design point. The trend indicates that changes in stator bore have a significant impact on the performance index; certain bore values result in better electromagnetic performance (higher efficiency or lower loss), while others degrade it. This figure essentially highlights the sensitivity of motor performance to stator bore size, assisting designers in choosing the bore that yields the best trade-off between torque, power factor, and efficiency. The orange lines connect design iterations, showing how the optimization algorithm navigated the search space, and the design point label indicates the optimal or selected solution among the valid designs. Figure 7 is the design point and yoke length. In this case, the y-axis shows the value of the objective function, and the x-axis shows the yoke length. Black points represent rejected or incorrect solutions, while red points represent workable designs, as in the previous picture. Since the yoke length directly affects flux route length, leakage flux, and magnetic saturation, the variation demonstrates that it has a considerable impact on magnetic performance. While a long yoke unnecessarily increases motor size and material expense, a short yoke length may result in core saturation. The optimization technique finds workable ranges where performance is maximized by experimenting with various yoke lengths. In order to ensure that the yoke length supports sufficient flux without oversizing the machine, the design point marker determines the optimal compromise solution.

The impact of stator width (also known as tooth width or slot width, depending on the situation) on the objective function is plotted in Figure 8. Stator width with design point. Black points represent faulty solutions, and red points represent verified designs, as in the other representations. Stator width affects winding accommodation, flux carrying capacity, and slot area (and thus current density). A stator that is too wide leaves less room for windings, which lowers ampere-turns and, consequently, torque, whereas a stator that is too narrow can overheat in applications because of high current density. Only a portion of the achievable performance envelope is contained within the scatter distribution, which displays a broad range of potential configurations. The ideal stator width that balances torque production, efficiency, and temperature restrictions is indicated by the chosen design point.

Figure 9 shows the design point; the rotor diameter (x-axis) and the objective performance function (y-axis) are plotted. Validated designs, or workable solutions that satisfy all requirements, are shown by red points. Invalid or non-converged designs (constraint violations) are indicated by black points. The optimization algorithm's exploration path is traced by the orange connecting lines, which demonstrate how solutions changed over iterations. The ideal rotor diameter that offers the best balance between efficiency, torque, and temperature restrictions is indicated by the chosen design point. The distribution of points demonstrates that torque generation

and leakage flux are significantly impacted by rotor diameter. Reduced air-gap area and flux linkage result in lesser torque in applications with too narrow a rotor diameter. An excessively large rotor diameter may result in mechanical or thermal stress, increased leakage flux, and increased inertia. Therefore, the optimization aids in determining the ideal rotor diameter that prevents mechanical oversizing while balancing thermal and electromagnetic performance**.** Figure 10: Design point and stator bore; the impact of the stator bore (x-axis) on the objective function (y-axis) is investigated in this image. Similar to the last illustration, black points indicate designs that are invalid or impractical, and red points indicate designs that have been validated as workable. The trade-off boundary along which performance is maximized under specified limitations is indicated by the orange Pareto front. The variety of designs demonstrates that the stator bore dimension has a significant impact on Air-gap length (which influences torque output and flux density). magnetic loading (a larger bore may decrease the flux concentration). Thermal performance (copper space factor and heat dissipation are affected by bore size). The ideal stator bore that guarantees efficient flux distribution, high efficiency, and lower core losses is indicated by the design point marker. The spread of invalid (black) designs outside practical ranges is due to poor electromagnetic performance caused by incorrect bore sizing, which can be either too small or too large. In figure 11, the black dot represents a design or solution evaluated during the optimization process. Thus, the Pareto front is indicated by the red dot, which consists of non-dominated solutions. These are the "best possible trade-offs"; one cannot improve one objective without degrading the other. Green crosses: Indicate validated designs. These are designs that have been verified through detailed simulation or testing (higher fidelity models). They're sparse, suggesting only a few solutions were fully validated for the best model

Table 2.0: Summary of motor performances

Parameter	Normal Design	Single Objective	Multi-Objective
Efficiency	75%	85%	90%
Starting Torque	22.2 Nm	59Nm	68Nm
Starting Current	14A	20A	22A
Power Factor	0.85	0.90	0.90
Losses	116W	102W	89W

Table 3.0: Design and optimized Variable values

Variables	Initial Design Values	Optimized Values
Stator slot (Ds)	18	18
Stator length (Ls)	90	72.2
Number of turns (N)	50	55
Wire diameter (Wd)	1.1	0.911
Rotor bar (Dr)	80	76.5

Table 4.0: Motor performance requirements for multi-objective optimization

parameters	Efficiency (%)	Torque (Nm)	Losses (W)	Power Factor	Constraint	Currents (A)
Efficiency (%)	Targeted efficiency	≥ load torque	Min losses	High	≤85%	≤ 8-10
Torque (Nm)	High Efficiency	Targeted Torque	Min Losses	High P.F	≥ Required load	Min Current draw
Currents (A)	High Efficiency	Acceptable torque	Min Losses	Moderate Pf	≥5≥10	Min Current draw
Power Factor	High Pf	≥ Design Load	Min Losses	High P. F	≥ Required load	≤ 10
Size	High Eff.	≥ Required Torque	Min Losses	High PF	≥ Required Size	≤ 10

Important performance metrics utilized in the design and optimization of an induction motor include efficiency, torque, power factor, losses, current, and motor size. Each of these factors influences the machine's overall mechanical, thermal, and electromagnetic behavior and serves as both a design goal and a restriction. The motor performance criteria for multi-objective optimization of an induction motor are compiled in Table 4. Whether the optimization is single-objective or multi-objective, this is essential for electric machines.

V. Conclusion

This work offered a thorough multi-objective design and optimization strategy for a three-phase induction motor (IM), especially optimized for traction applications. The research effectively addressed the competing objectives commonly found in traction motor design, namely, optimizing efficiency and torque while minimizing losses, volume, and temperature rise by combining electromagnetic, thermal, and performance-based design equations with cutting-edge optimization techniques like Particle Swarm Optimization (PSO). Finding a Pareto-optimal front was made possible by the multi-objective optimization framework, which provided a variety of trade-off options amongst performance metrics, including torque density, efficiency, power factor, and thermal

safety. In traction applications, where great torque, compactness, and energy economy are all required at the same time under different load circumstances, these trade-offs are especially important. The enhanced designs considerably exceeded baseline configurations in terms of electromagnetic performance, thermal behavior, and operating efficiency, according to simulation and analytical results. Furthermore, the outcomes showed how well PSO handled the multidimensionality, complexity, and nonlinearity included in traction motor design issues.

Declarations

Ethical Approval: This research did not include human subjects or animals. All data utilized were sourced from secondary sources, simulation models, and publicly accessible system parameters; hence, ethical approval was unnecessary for this study.

Consent To Participate: Consent to participate was not required.

Consent To Publish: Consent to publish was not required.

Data Availability: The datasets generated during and/or analyzed during the current study are available from the corresponding author on reasonable request.

Competing Interests: The authors declare that they have no competing interests related to the content of this manuscript

Funding: Not Applicable

Authors' Contributions

1. **Asuquo Eke:** Conceptualization, Methodology, Data curation, Analysis and Writing
2. **O. I. Okoro:** Review, Editing and Supervision
3. **A. J. Onah:** Review, Editing and Supervision

Acknowledgements: Not Applicable

References

[1] Okoro, O. I. Steady State And Transient Analysis Of Induction Motor Driving A Pump Load. Nigerian Journal Of Technology, 22(1), 46-53.2003

[2] Eke, A., Fischer, G., David, A., Ekpenyong, O., & E.J, Akpama. The Effect Of Rotor And Stator Slot Numbers On The Performance Of Three-Phase Induction Motors Used For Transport Application. IOSR Journal Of Electrical And Electronics Engineering (IOSR-JEEE). Volume 19, Issue 4 Ser. 1 (July. – August. 2024), PP 01-09. 2024

[3] Riviére N., M. Villani And M. Popescu, "Optimization Of A High-Speed Copper Rotor Induction Motor For A Traction Application," IECON 2019 - 45th Annual Conference Of The IEEE Industrial Electronics Society, Lisbon, Portugal, 2019, Pp. 2720-2725, Doi: 10.1109/IECON.2019.8927627

[4] Zhang M, Guo L., And H. Wang, "AI-Based Torque Estimation For Induction Motors Using LSTM Networks," *IEEE Transactions On Industrial Informatics*, Vol. 18, No. 3, Pp. 1950–1960, 2022.

[5] Schofield N., A. Boglietti, And A. Cavagnino, "Thermal Analysis Of Traction Motors: Cooling Technologies For High Torque Density Machines," *IEEE Transactions On Industry Applications*, Vol. 48, No. 5, Pp. 1565–1574, 2012.

[6] Popescu M., D. A. Staton, And T. J. E. Miller, "Thermal Analysis Of Electric Machines With Integrated Drive Cycles," *IEEE Transactions On Industry Applications*, Vol. 54, No. 5, Pp. 5168–5178, 2018.

[7] Kumar R. Singh, And P. Sharma, "CNN-Based Fault Detection In Induction Motors," *IEEE Transactions On Instrumentation And Measurement*, Vol. 72, Pp. 1–10, 2023.

[8] Baroudi M, A. M. Shirdel, And R. Mcmahon, "Design Of Deep-Bar Induction Motors For Evs," Presented At The IEEE ICEM 2021 Conference.

[9] Silva E. M. "Multi-Objective Optimization Of Squirrel Cage Rotor For Electric Vehicle Induction Motor Using NSGA-II," IEEE Trans. Magn., Vol. 53, No. 6, 2017.

[10] Momeni A., "Multi-Objective Optimal Design Of Ims For Traction: Torque Density And Cost Trade-Off," Electr. Power Syst. Res., Vol. 180, 2020.

[11] Jiang F., "MOPSO-Based Optimal Control Of Induction Motor Drives In Electric Vehicles," IEEE Access, Vol. 7, 2019.

[12] Zhang T. "Intelligent Torque Control Of Induction Motor For Evs Using MOO And Neural Networks," IEEE Trans. Ind. Electron., Vol. 69, No. 4, 2022.

[13] Popescu N.., "Coupled Electromagnetic And Thermal Optimization Of Traction Motors," IEEE Trans. Ind. Appl., Vol. 54, No. 5, 2018.

[14] Yildirim S., "Surrogate-Assisted MOO Of Thermal Design For Traction Motors," Appl. Therm. Eng., Vol. 192, 2021.

[15] Asuquo E., Koledoye T. O, Osokoya S. O., Akpama E. J., Comparative Analysis And Evaluation Of Induction Motor Transient Behaviour On Different Loading Conditions, International Journal Of Innovative Science, Engineering & Technology, Vol. 8 Issue 9, September 2021 ISSN (Online) 2348 – 7968 | Impact Factor (2020) – 6.72 2021

[16] Barri, D., Soresini, F., Gobbi, M., Di Gerlando, A. And Mastinu, G. Optimal Design Of Traction Electric Motors By A New Adaptive Pareto Algorithm. IEEE Transactions On Vehicular Technology. 2025

[17] Khan, S.A., Bhowmick, S. And Singh, M. Design Of Switched Reluctance Motor For Light Electric Vehicles Using Multi-Objective Driving Training-Based Optimization Algorithm. Arabian Journal For Science And Engineering, Pp.1-22. 2025

[18] Cvetkovski, G. And Petkovska, L. Design Improvement Of Permanent Magnet Motor Using Single And Multi-Objective Approach. Power Electronics And Drives, 9, Pp.34-49. 2024

[19] Roshandel, E., Mahmoudi, A., Soong, W.L. And Kahourzade. Optimal Design Of Induction Motors Over Driving Cycles For Electric Vehicles. IEEE Transactions On Vehicular Technology, 72(12), Pp.15548-15562. 2023

[20] Sun, C., Li, Q., Fan, T., Wen, X., Li, Y. And Li, H. Multi-Objective Optimal Design Of 200 Kw Permanent Magnet Synchronous Motor Based On NSGA-II. World Electric Vehicle Journal, 16(6), P.299. 2025